#4122

(12) Aston, S. R.; Stanners, D. A. *Nature* **1981**, *289*, 581–582.
(13) Beasley, T. M.; Carpenter, R.; Jennings, D. C. *Geochim. Cosmochim. Acta* **1982**, *46*, 1931–1946.
(14) Scott, M. R.; Salter, P. F.; Halverson, J. E. *Earth Planet. Sci. Lett.* **1983**, *63*, 202–222.
(15) Santschi, P. H.; Li, Y.-H.; Bell, J. J.; Trier, R. M.; Kawtaluk, K. *Earth Planet. Sci. Lett.* **1980**, *51*, 248–265.
(16) Aston, S. R.; Assinder, D. J.; Kelly, M. *Estuarine, Coastal Shelf Sci.* **1985**, *20*, 761–771.
(17) Smith, J. N.; Boudreau, B. P.; Noshkin, V. *Earth Planet. Sci. Lett.* **1987**, *81*, 15–28.
(18) Sholkovitz, E. R.; Mann, E. R. *Estuarine, Coastal Shelf Sci.* **1987**, *25*, 413–434.
(19) Linsalata, P.; Wrenn, M. E.; Cohen, N.; Singh, N. P. *Environ. Sci. Technol.* **1980**, *14*, 1519–1523.
(20) Kuehl, S. A.; DeMaster, D. J.; Nittrouer, C. A. *Cont. Shelf Res.* **1986**, *6*, 209–225.
(21) Hayes, D. W.; Sackett, W. M. *Estuarine, Coastal Shelf Sci.* **1987**, *25*, 169–174.
(22) Pinder, J. E., III; Paine, D. In *Transuranic Elements in the Environment*; Hanson, W. C., Ed.; U.S. Department of Energy: Springfield, VA, 1980; pp 165–172.
(23) Alberts, J. J.; Halverson, J. E.; Orlandini, K. A. *J. Environ. Radioact.* **1986**, *3*, 249–271.
(24) Hardy, E. P.; Krey, P. W.; Volchok, H. L. *Nature* **1973**, *241*, 444–445.
(25) Olsen, C. R.; Larsen, I. L.; Lowry, P. D.; McLean, R. I.; Domotor, S. L. Radionuclide Distributions and Sorption Behavior in the Susquehanna–Chesapeake Bay System. Maryland Power Plant and Environmental Review PPER-R-12; Annapolis, MD, 1989.
(26) Marter, W. L. Radioactivity from SRP Operations in a Downstream Savannah River Swamp. Atomic Energy Commission Report DP-1370. E. I. du Pont de Nemours Co.: Aiken, SC, 1974.
(27) Mulholland, P. J.; Olsen, C. R. submitted for publication in *Estuarine, Coastal Shelf Sci.*
(28) Krishnaswami, S.; Benninger, L. K.; Aller, R. C.; Von Damm, K. L. *Earth Planet. Sci. Lett.* **1980**, *47*, 307–318.
(29) Olsen, C. R.; Larsen, I. L.; Lowry, P. D.; Cutshall, N. H.; Nichols, M. M. *J. Geophys. Res.* **1986**, *91*, 896–908.
(30) Craig, H. *Geochim. Cosmochim. Acta* **1953**, *3*, 53–92.
(31) Gearing, J. N.; Gearing, P. J.; Rudnick, D. T.; Requejo, A. G.; Hutchins, M. J. *Geochim. Cosmochim. Acta* **1984**, *48*, 1089–1098.
(32) Hedges, J. I.; Parker, P. L. *Geochim. Cosmochim. Acta* **1976**, *40*, 1019–1030.
(33) Krom, M. D.; Bennett, J. T. *Estuarine, Coastal Shelf Sci.* **1985**, *21*, 325–326.
(34) Turekian, K. K.; Benoit, G. J. In *Flux of Organic Carbon by Rivers to the Oceans*. U.S. Department of Energy: Washington, DC, 1981; DOE/OER CONF-8009140, pp 314–330.
(35) Thein, M.; Ballestra, S.; Yamato, A.; Fukai, R. *Geochim. Cosmochim. Acta* **1980**, *44*, 1091–1097.
(36) Cutshall, N. H.; Larsen, I. L.; Olsen, C. R. *Nucl. Instrum. Methods* **1983**, *206*, 309–312.
(37) Hamilton-Taylor, J.; Kelly, M.; Mudge, S.; Bradshaw, K. *J. Environ. Radioact.* **1987**, *5*, 409–423.
(38) Shen, G. T.; Sholkovitz, E. R.; Mann, E. R. *Earth Planet. Sci. Lett.* **1983**, *64*, 437–444.

Received for review November 9, 1988. Accepted June 29, 1989. This research was sponsored by the Ecological Research Division, Office of Health and Environmental Research, U.S. Department of Energy, under contract DE-AC05-840R21400 with the Martin Marietta Energy Systems, Inc., and under contract DE-FG09-86-ER60435 with Skidaway Institute of Oceanography. Publication No. 3341, Environmental Sciences Division, Oak Ridge National Laboratory.

Modeling and Field Evidence of Pressure-Driven Entry of Soil Gas into a House through Permeable Below-Grade Walls

Karina Garbesi* and Richard G. Sextro

Indoor Environment Program, Lawrence Berkeley Laboratory, University of California, Berkeley, California 94720

■ Modeling and field evidence are presented that indicate that soil gas can enter houses with basements at significant rates through permeable below-grade walls. Entry via this pathway could result in elevated indoor concentrations of radon and other pollutants. By use of artificial depressurization of the basement (−25 to −30 Pa), field measurements were made of pressure coupling between a basement and the surrounding soil and of soil-gas entry into the house. A two-dimensional, steady-state finite element model of fluid flow through porous media was used to simulate the experimental conditions, assuming air flow occurs through permeable substructure walls. Given a basement wall permeability consistent with prior experimental research, the model predicts 32% pressure coupling 0.5 m from the basement wall at a depth of 0.5 m, in agreement with pressure coupling measured at the site. Under the same conditions the model predicts a soil-gas entry rate of 2.5 $m^3\ h^{-1}$, within the range estimated by tracer-gas measurements. The presence of a horizontal, low-permeability soil layer just above basement floor level explains the high pressure coupling observed at 3-m depth even out to 14 m west of the house.

Introduction

Soil gas is an important source of indoor air pollution. Research on sources of human exposure to radon indicate that soil is the primary source of indoor radon in single-family houses in the United States (*1*). Pressure-driven flow is a principal means by which soil gas enters houses; it is expected to be the predominant source of radon in houses with elevated concentrations (*2–4*). Recent studies indicate that entry of volatile organic contaminants via the soil-gas pathway could pose a public health risk in residences located near landfills, even those designed to accept only nonhazardous waste (*5, 6*).

Pressure-driven flow of soil gas into houses results from the depressurization of the substructure of the house with respect to the surrounding soil. There are three principal causes of basement depressurization: thermal differences between indoors and outdoors, wind loading on the building superstructure, and imbalanced building ventilation (*2, 4*). Field measurements have shown that under normal operating conditions of houses during the winter the temperature effect alone can result in consistent substructure underpressures of between 2 and 6 Pa (*7, 8*). Other factors being equal, pressure-driven entry is likely to be most important in houses with basements because they provide a large interface with the soil. Soil-gas entry due to basement depressurization has been experimentally demonstrated by Turk et al. (*9*) and Nazaroff et al. (*10*). Significant pressure-driven entry of radon from soil has also been reported for houses with crawl spaces (*11*). Entry pathways have been assumed to be penetrations, gaps, or

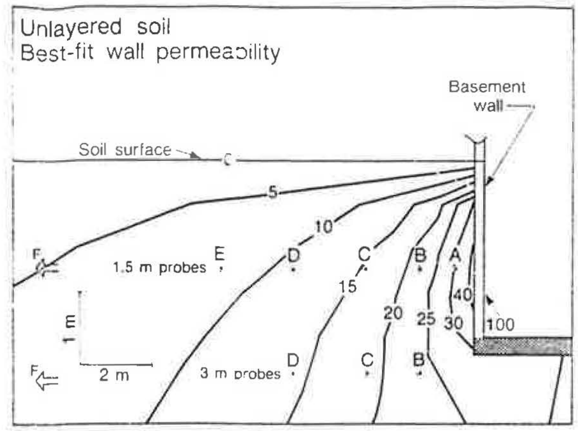

gure 2. Pressure contour map generated by the finite element model r the case of unlayered soil and best-fit wall permeability (case 8, on). Pressure contours are given in percent of basement unrpressure. Soil probe locations are marked by bull's-eyes.

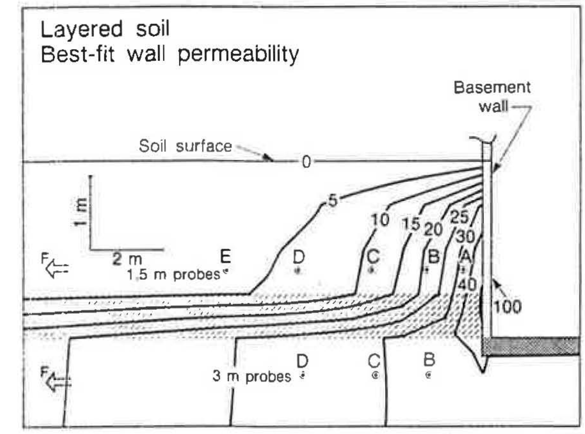

gure 3. Pressure contour map generated by the finite element model r the case of layered soil and best-fit wall permeability (case 9, Lbn). ie shaded area indicates the low-permeability soil layer. Pressure ontours are given in percent of basement underpressure. Soil probe cations are marked by bull's-eyes.

and D decreases with decreasing wall permeability as oes the vertical pressure gradient between the soil surface nd the A-row probe. By Darcy's law, this reduced presire gradient results in decreased soil-gas flow rates.

The addition of the low-permeability soil layer has little fect on near-house pressure coupling above the depth of ie layer. Far-field coupling below the layer is, however, eatly increased in the presence of the layer (compare igures 2 and 3). This phenomenon accounts for the high essure coupling observed at 3-m-deep probes in the C–E ws (Figure 1), whereas the homogeneous soil model does ot (for example, Figure 2). The net effect of the low ermeability layer is to extend the zone of influence of the ouse in the deep soil. This effect, in combination with ie leakage geometry of the house substructure, can be an nportant determinant of soil contaminant entry rates. specially since most sources would be expected, in the esence of a low-permeability soil layer, to have higher incentrations in deeper soil because of reduced dilution surface air.

A comparison of cases 6, 7, and 10 with cases 4, 5, and respectively (Table II), shows that the presence of the ickfill region, as modeled, has little effect on predicted essure coupling. (The pressure contour map for the ickfill case is almost identical with Figure 3.) For a given ıll permeability, all soil configurations produce similar sults in the near-field above the depth of the soil layer. ıis result would not be expected if the permeability of

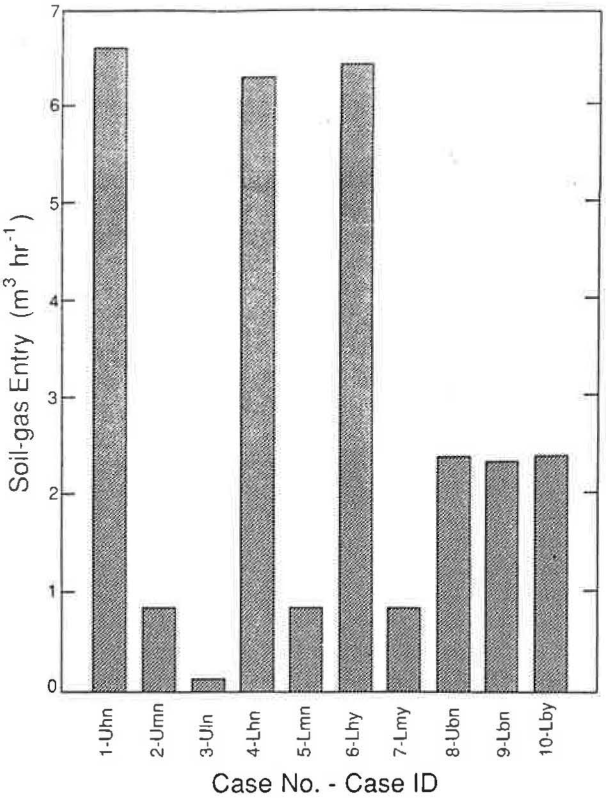

Figure 4. Entry rate of soil gas into the basement predicted by the finite element model for a basement pressure of −30 Pa. (See Table I for explanation of case number and ID.)

the backfill region was appreciably different from that of the bulk soil. For example, a very high permeability backfill zone should create a short circuit in the soil-gas flow path, reducing far-field coupling and flow.

A wall permeability of 9×10^{-14} m^2 gave a best fit to the measured pressure coupling averaged over each row (Tables I and II). This value is close to the permeability of 2×10^{-13} m^2 of cement-block material coated with a mortar sealant estimated from the results of Marynowski's (*18*) tests of air-flow through cement block walls. Although Marynowski's measurements were made on hollow block walls, a permeability can be calculated for the building material, subtracting out the effect of the void spaces by calculating an effective path length for air flow through the solid medium.

The model was run using the "best fit" wall permeability for all soil configurations: namely, for unlayered soil, layered soil, and layered soil with a backfill (cases 8–10, respectively). The pressures predicted for rows A–D at 1.5-m depth are presented in Table II. It is difficult to pick the best fit among the models from these data. However, as mentioned earlier, the high pressure coupling measured in 3-m-deep probes even out to 14 m from the house is approximated only by the layered-soil model.

Also shown in Table II are predictions from the finite difference models of Mowris (*13*) and Loureiro (*14*) for the A–D-row locations for 1- and 10-mm wall–floor gap widths, for the case of homogeneous soil. Even for a gap as large as 10 mm, these models clearly underpredict pressure coupling at this site. Whereas, with a reasonable wall permeability of 9×10^{-14} m^2, the permeable wall model yields fairly accurate predictions. This result indicates that it is likely that entry occurred distributed over the wall area.

Figure 4 plots the soil-gas entry rate based on the current model for each of the 10 cases considered. The output of the model is given in volumetric flow rate per unit of horizontal wall length (the third dimension not included in the model) associated with each flux–boundary node. To estimate the rate of soil-gas flow into the basement, the sum of the wall fluxes are simply multiplied by the length of the wall adjoining the soil, the flux through the floor slab being negligible. The results indicate that soil-gas entry is slightly less than proportional to wall permeability. As the wall permeability decreases, the entry rate should converge on being proportional to wall permeability, since the coupled resistance to flow presented by the soil and wall will be dominated by the wall.

Since the model specifies that soil-gas entry occurs along the entire depth of the wall, but the majority of the wall is above the low-permeability soil layer, the presence or absence of the layer has little effect on the entry rate (Figure 4). A quite different result would be expected if entry occurred primarily below the level of the soil layer (for example, if entry occurred through a gap at the wall–floor joint or through a permeable earthen floor). In that case, a low-permeability soil layer should obstruct the source of surface air, restricting soil-gas entry into the building.

Although the tracer-gas estimate of the soil-gas entry rate has fairly large range, and therefore a comparison with this estimate does not provide a rigorous test of the model, it is reassuring that the model prediction of entry rate falls within the range estimated by the tracer-gas technique. In cases 8–10 of Figure 4, using the wall permeability that gave a best fit to the pressure coupling data, the model predicts an entry rate of $\sim$2.5 m^3 h^{-1}. By contrast, a perimeter gap at the wall–floor interface cannot account for the measured entry, even assuming a large gap width. An analytical (closed form) model by Mowris and Fisk (*15*) was used for calculating soil-gas entry into a house via a gap at the wall–floor interface. With the geometric parameters of the study house, a basement depressurization of 30 Pa, and the average permeability of the bulk soil, the predicted soil-gas entry rate is 0.15 m^3 h^{-1} for a 1-mm gap width, and 0.20 m^3 h^{-1} for a 10-mm gap width, an order of magnitude below the measured value and the value predicted by the permeable wall model. This strongly suggests that, at the field site, entry occurred distributed over the wall area. This also suggests the importance that porous building materials might play in the entry of soil contaminants into houses. Even in houses that do have a wall–floor gap in the basement, transport through porous below-grade walls might dominate soil-gas entry.

It should be noted that because of the relatively low permeability of the soil at the study site, at normal basement underpressures soil-contaminant entry could be explained by either diffusion of convection. For more detail see Garbesi (ref 20, p 60). However, at sites with higher permeability soils, advective flow, driven by depressed basement pressures, should dominate. See, for example, ref 9. Our research suggests that, in sufficiently permeable soils, under normal house operating conditions, subsurface entry of soil gas into houses could be significantly elevated by transport through permeable walls.

Conclusions

This work demonstrates the potential importance of a previously neglected pathway for soil-gas entry into houses: pressure-driven flow through permeable, below-grade building materials. Such flow, distributed over the wall area, could occur via porous building materials or via a network of small cracks. If this pathway is ignored in modeling of soil-gas entry into buildings, predictions of the soil-gas entry rate could be substantially too low. For example, neglecting the permeable-wall pathway at the field site and assuming entry through a 10-mm gap at the wall–floor joint results in an order of magnitude underprediction of the soil-gas entry rate. Furthermore, in houses that do have a peripheral gap, entry through the gap could be small compared with entry through the walls.

A second factor, explored in a limited way, is the effect of a low-permeability soil layer just above basement floor level (such a layer was apparent at the field site). The layered-soil model predicts significantly higher far-field pressure coupling below the layer than does the homogeneous soil model and helps to explain the high pressure coupling observed at the 3-m depth even out to 14 m from the house.

These findings have important implications for assessing human exposures to contaminants with a soil-gas source, such as radon and volatile organic contaminants. Wall permeability affects the rate at which soil gas may enter a house. Layering of the soil can determine the region from which soil gas is drawn and, therefore, the concentration of the entering gas. Soil macrostructure also affects the shape of the pressure field, thereby determining the zone of influence of the house and the strength of pressure coupling in different regions. These factors are crucial for understanding and predicting concentrations of contaminants in indoor air.

The results of this study also have bearing on indoor air pollution mitigation techniques. Entry through walls could explain why the sealing of gaps and penetrations in building substructures has been found to be relatively ineffective as a radon-entry mitigation measure (*9*). This research supports the idea that impermeable wall coatings might be a useful mitigation technique, reducing the need for such methods as basement overpressurization, subslab depressurization, or crawl-space ventilation. The use of impermeable sealants as a technique for reducing radon entry has been discussed (*17*), but entry via permeable walls has been investigated only in a limited way and the relative importance of soil-gas entry via this pathway is unknown.

More research is needed in order to determine the magnitude and frequency of soil-gas entry through permeable building materials in the existing housing stock. More data are needed on the permeability of various building materials and sealants. In particular, tests should be made on constructed walls, such as cement-block walls sealed and backfilled with cement. With data such as these, and with information on current building design, modeling could be used more effectively to assess the magnitude of soil-gas entry in the existing housing stock. These studies could, in turn, be used to help ensure that future building practices reduce indoor air pollution by limiting soil-gas entry.

Acknowledgments

We thank Nicholas Sitar for providing the finite element model. We are grateful for the editorial comments of Al Hodgson, Joan Daisey, William Nazaroff, William Fisk, and Nicholas Sitar.

Registry No. Radon, 10043-92-2; Freon 12, 75-71-8; SF_6, 2551-62-4.

Literature Cited

(1) Nero, A. V.; Nazaroff, W. W. *Radiat. Prot. Dosim.* **1984**, 7, 23–39.

(2) DSMA Atcon Ltd. *Review of Existing Information and Evaluation for Possibilities of Research and Development of Instrumentation to Determine Future Levels or Radon at a Proposed Building Site*; Atomic Energy Control Board:

Ottawa, Ontario, Canada, 1983; INFO-0096.
(3) Sextro, R. G.; Moed, B. A.; Nazaroff, W. W.; Revzan, K. L.; Nero, A. V. In *Radon and Its Decay Products: Occurrences, Properties, and Health Effects*; Hopke, P., Ed.; ACS Symposium Series 331; American Chemical Society: Washington DC, 1987; Chapter 2.
(4) Nazaroff, W. W.; Moed, B. A.; Sextro, R. G. In *Radon and Its Decay Products Indoors*; Nazaroff, W. W., Nero, A. V., Eds.; Wiley: New York, 1988; Chapter 2.
(5) Wood, J. A. Porter, M. L. *J. Air Pollut. Control Assoc.* **1987**, *37*, 609-615.
(6) Hodgson, A. T.; Garbesi, K.; Sextro, R. G.; Daisey, J. M. *J. Air. Pollut. Control Assoc.*, in press.
(7) Turk, B. H.; Prill, R. J.; Fisk, W. J.; Grimsrud, D. T.; Moed, B. A.; Sextro, R. G. *Radon and Remedial Action in Spokane River Valley Homes*; Lawrence Berkley Laboratory: Berkeley, CA, 1987; Vol. 1, LBL-23430.
(8) Turk, B. H.; Prill, R. J.; Sextro, R. G.; Harrison, J. In *Proceedings of the 1988 Symposium on Radon and Radon Reduction Technology*; Denver, CO; U.S. Environmental Protection Agency: Denver, CO, 1988; Paper No. VI-3.
(9) Turk, B. H.; Prill, R. J.; Fisk, W. J.; Grimsrud, D. T.; Moed, B. A.; Sextro, R. G. In *Proceedings of the 79th Annual Meeting of the Air Pollution Control Association*; Minneapolis, MN; Air Pollution Control Association: Pittsburgh, PA, 1986; Paper No. 86-43.2.
(10) Nazaroff, W. W.; Lewis, S. R.; Doyle, S. M.; Moed, B. A.; Nero, A. V. *Environ. Sci. Technol.* **1987**, *21*, 459-466.
(11) Nazaroff, W. W.; Doyle, S. M. *Health Phys.* **1985**, *48*, 265-281.
(12) Nazaroff, W. W.; Feustel, H.; Nero, A. V.; Revzan, K. L.; Grimsrud, D. T.; Essling, M. A.; Toohey, R. E. *Atmos. Environ.* **1985**, *19*, 31-46.
(13) Mowris, R. J. *Analytical and Numerical Models for Estimating the Effect of Exhaust Ventilation on Radon Entry in Houses with Basements or Crawl Spaces*; Lawrence Berkeley Laboratory: Berkeley, CA, 1986; LBL-22067.
(14) Loureiro, C. O. *Simulation of the Steady-state Transport of Radon from Soil into Houses with Basements under Constant Negative Pressure*: Lawrence Berkeley Laboratory: Berkeley, CA, 1987; LBL-24378.
(15) Mowris, R. J.; Fisk, W. J. *Health Phys.* **1988**, *54*, 491-501.
(16) United States Environmental Protection Agency *A Citizen's Guide to Radon: What Is It and What Do We Do About It?*; United States Environmental Protection Agency: Washington, DC, August 1986; OPA-86-004.
(17) United States Environmental Protection Agency *Radon Reduction Methods: A Home Owners Guide*; United States Environmental Protection Agency: Washington, DC, August 1986; OPA-86-005.
(18) Marynowski, J. M. *Measurement and Reduction Methods of Cinder Block Wall Permeabilities*; Center for Energy and Environmental Studies: Princeton University, Princeton, NJ, 1988; Working Paper No. 99.
(19) Harris, B. B.; Ruppersberger, J. S.; Walton, M. Presented at 1988 Symposium on Radon and Radon Reduction Technology; Denver, CO; U.S. Environmental Protection Agency, Denver, CO, October 1988.
(20) Garbesi, K. *Experiments and Modeling of the Soil-Gas Transport of Volatile Organic Compounds into a Residential Basement*; Lawrence Berkeley Laboratory: Berkeley, CA, 1988; LBL-25519 Rev.
(21) Hillel, D. *Fundamentals of Soil Physics*; Academic Press: New York, 1980; Chapter 11.
(22) Conner, J. J.; Brebbia, C. A. *Finite Element Techniques for Fluid Flow*; Newnes-Butterworths: Boston, MA, 1976.

Received for review March 16, 1989. Accepted August 17, 1989. This work was supported by the Occidental Chemical Corp. under Agreement BG 8602A and by the Assistant Secretary for Conservation and Renewable Energy, Office Building and Community Systems, Building Systems Division of the U.S. Department of Energy under Contract DE-AC03-76SF00098.

A Shrouded Aerosol Sampling Probe†

Andrew R. McFarland,* Carlos A. Ortiz, Murray E. Moore, Robert E. DeOtte, Jr., and Sriram Somasundaram

Department of Mechanical Engineering, Texas A&M University, College Station, Texas 77843

■ A new device—a shrouded probe—has been developed for sampling aerosol particles from moving airstreams. In its design, a 30-mm-diameter sampling probe is located concentrically within a 105-mm-diameter, cylindrically shaped shroud. The flow rate through the sampling probe is a constant value of 170 L/min. The dynamic pressure of the external airstream forces flow through the region between the shroud and the internal probe. The velocity of air in the shroud is 0.40 that of the free stream over a wide range of free stream velocities (2-14 m/s). The wall losses of 10-μm particles in the shrouded probe operated at 170 L/min in a 14 m/s airstream are 13% as compared with 39% for an isokinetic probe. Wind tunnel experiments with 10-μm-diameter particles over the range of free stream velocities of 2.0-14 m/s and a flow rate of 170 L/min show the transmission ratio for the shrouded probe to be within the range of 0.93-1.11.

Introduction

The standard approach to obtain a representative sample from a moving gas stream in a flow duct is with an isokinetic probe (*1-3*). Considerable research has characterized the effects of sampling with isokinetic probes under conditions that are either anisokinetic or in which the probe is aligned at off-axis angles, e.g., probe at nonzero pitch or yaw angles relative to the moving airstream (*4-8*).

Two parameters describe the efficacy of a sampling probe: the aspiration coefficient, A, and the transmission ratio, T. The aspiration coefficient gives the ratio of the spatial mean concentration at the probe inlet, C_p, to the concentration in the free stream, C_0, i.e.:

$$A = C_p/C_0 \tag{1}$$

The aspiration coefficient can be represented functionally as

$$A = f(\mathrm{St}, \mathrm{Re}, U_0/V_p, \alpha, \theta) \tag{2}$$

where St is the Stokes number ($C\rho_p D_p^2 U_0/9\mu d$), and Re is the probe Reynolds number ($\rho U_0 d/\mu$). C is the Cunningham correction for slip flow (approximately unity for particles that exhibit anisokinetic sampling effects), ρ_p is the particle density, D_p is the particle diameter, U_0 is the free stream velocity, μ is the fluid viscosity, d is the diameter of the probe inlet, ρ is the fluid density, V_p is the spatial mean velocity at the probe inlet plane, and α and

†Aerosol Technology Laboratory Publication 5897/01/09/88/ARM.

0013-936X/89/0923-1487$01.50/0

Table I. Descriptions of Each Case of the Finite Element Model Specifying Case Identification (ID) and Wall Permeability

case no.	case description			case ID[d]	wall perm, m²
	soil[a]	wall[b]	backfill[c]		
1	unlayered	high	no	Uhn	3×10^{-13}
2	unlayered	medium	no	Umn	3×10^{-14}
3	unlayered	low	no	Uln	3×10^{-15}
4	layered	high	no	Lhn	3×10^{-13}
5	layered	medium	no	Lmn	3×10^{-14}
6	layered	high	yes	Lhy	3×10^{-13}
7	layered	medium	yes	Lmy	3×10^{-14}
8	unlayered	best fit	no	Ubn	9×10^{-14}
9	layered	best fit	no	Lbn	9×10^{-14}
10	layered	best fit	yes	Lby	9×10^{-14}

[a] Soil configuration unlayered or layered. [b] Wall permeability: high, medium, low, or "best fit". [c] Backfill: yes, if present; no, if absent. [d] Case ID designated by the first letter of the soil, wall, and backfill descriptions.

Table II. Pressure Coupling at 1.5-m Depth[a]

case no.	case ID[b]	row designation (distance from house, m)			
		A (0.5)	B (1.5)	C (3.0)	D (5.0)
			Range		
1	Uhn	50	36	25	18
2	Umn	19	13	9	7
3	Uln	6	4	3	2
4	Lhn	51	34	18	10
5	Lmn	20	13	7	4
6	Lhy	52	36	19	10
7	Lmy	22	14	7	4
			Best Fit		
8	Ubn	31	22	15	11
9	Lbn	32	21	12	6
10	Lby	33	23	12	6
			Field Data[c]		
		32	21	13	10
			Other Models		
Mowris (1 mm)		11	8	5	3
Mowris (10 mm)		11	10	6	4
Loureiro (1 mm)		8	6	4	2
Loureiro (10 mm)		12	8	6	3

[a] Predicted by the permeable wall model used here and by perimeter gap models of other authors, and averaged pressure coupling determined by field measurements. All table values are percentages of basement depressurization. The table is divided into four sections designated as follows: range, best fit, data, and other models. Range: represents cases that present the range of wall permeabilities, corresponding to the first seven cases of Table I. Best fit: corresponds to the last three cases in Table I, where the wall permeability is picked to produce a best fit to the field data. Other models: gives the pressure coupling predicted by the numerical models of Mowris (13) and Loureiro (14) for a basement wall–floor gap width of 1 and 10 mm. [b] See Table I for explanation of case ID. [c] Data values are the average value for 1.5-m deep, west-side probes in each row. One data point on the northwest corner of the house with 4% coupling was omitted from the data set as an obvious outlier (see Figure 1).

10%. Given the idealization implicit in the assumptions governing the input to the model, this level of error is tolerable. That is, actual deviations at the site from the assumptions of a homogeneous wall and regionally homogeneous soil are likely to result in uncertainties at least this large.

To quantify the effect of basement wall permeability on soil-gas entry, the permeability of the wall was varied among the cases modeled. Table I summarizes the permeabilities assigned to the wall elements in each of the 10 cases. Results are presented for permeabilities ranging from 3×10^{-13} to 3×10^{-15} m². Uncracked poured slab is known to be significantly less permeable than cement block. For modeling convenience the cement-slab floor was assigned a low permeability of 3×10^{-20} m². This choice effectively limits entry to the wall area.

The permeable wall model applies to flow through uniform porous media (for example to homogeneously porous building materials), to flow through a composite wall made up of different material types, or to flow through numerous small cracks in the cement block, the mortar, or both. In the latter two cases an effective permeability for the wall can be assigned as long as the channels through which flow occurs are small compared with the area over which flow is distributed. This is a common practice in hydrology when considering groundwater flow through a composite medium and in geology when considering fluid flow through cracks and fissures in rock. Therefore, in the current study *wall permeability* should be interpreted as the estimated effective permeability of the wall.

Since the groundwater table at the site was known to be approximately 20 m below the surface, the soil was assumed to be unsaturated throughout the modeled region. Three configurations of the soil were modeled. In one case, the soil was specified as being uniform throughout, with a permeability of 3×10^{-12} m² (the average measured permeability of the bulk soil). The second case tested the effect of a low-permeability soil layer just above basement floor level by assigning a permeability of 3×10^{-14} m² to the soil between 1.8- and 2.4-m depth, while the bulk of the soil was treated as in the first case. The permeability for this layer was based on the soil particle-size analysis. The depth approximates that estimated in the field and was chosen for modeling convenience. The low-permeability soil layer was terminated 17 m to the west of the house because at greater distances the elements of the mesh were not fine enough to define such a thin layer. Termination of the layer at this distance will not result in distortion of the pressure field within 5 m of the house, the region for which we make a quantitative comparison with the data. The results will be less reliable for F-row probes, 14 m west of the house.

The third soil configuration tests the effect of incorporating a region with potentially distinct soil permeability next to the basement wall. Such a region can result from the process of backfilling the house excavation hole with soil after completion of basement construction. In the case of the field site, permeabilities measured in the backfill zone were similar to those in the bulk soil, but higher than those in the low-permeability layer. Therefore, for the backfill case, soil permeabilities were specified as for the layered-soil case except that the low-permeability layer was terminated 1.0 m from the house, the soil between 0.0 and 1.0 m being assigned the permeability of the bulk soil. The soil is assumed to be homogeneous and isotropic within each region.

Discussion of Modeling Results

Table II presents the model predictions of pressure coupling (in percent of basement underpressure). A comparison of cases 1–3 demonstrates the effect of decreasing wall permeability on pressure coupling in the soil. As expected, pressure coupling decreases with decreasing wall permeability. In homogeneous soil, a reduction of wall permeability from 3×10^{-13} to 3×10^{-15} m² results in a reduction of predicted pressure coupling from 50 to 6% in the A row and from 18 to 2% in the D row. A similar trend can be seen for cases in which the soil is layered, and layered and backfilled (cases 4 and 5, and 6 and 7, respectively). The horizontal pressure gradient between rows ıcreasing distance out to 5 m from the house. At distances reater than 5 m, coupling showed a sudden increase. This 'as probably due to irregularity in the large-scale structure f the soil, with increased coupling reflecting a zone of ıcreased permeability between the basement and the far ield. Because the simple soil geometries modeled in this tudy will not predict such variation, we make quantitative omparisons between the model and the data only out to · m from the house. The comparison is made for probes ıf 1.5-m depth since the greater number of measurements ıt this depth provided better characterization of the ›ressure coupling between the basement and the soil.

Air-permeability measurements of the soil were also nade at all of the probes. The technique is described in letail in ref 20. On the basis of resistance during probe nsertion, there appeared to be a dense, hard layer ap- ›roximately one-half m thick lying between 2- and 3-m lepth, depending on probe location. Probes were generally erminated either above or below this layer because within he layer excessive resistance to air flow made permeability neasurements impossible with the available equipment. Therefore, mean permeabilities calculated from the in situ neasurements apply to the bulk soil, but not to the low- permeability layer. The mean permeability of the bulk soil (above and below the low-permeability layer) was 3×10^{-12} m^2 with a range of $(0.3-20) \times 10^{-12}$ m^2. Permeability of the soil in the dense layer was estimated by an indirect method. Soil samples were collected by bucket auger and analyzed for particle size distribution to determine the USDA soil type. Samples taken from the layer were of the silt-loam type, associated with an air permeability range of $10^{-14}-10^{-13}$ m^2 (*4*). Samples taken from the bulk soil were of the sandy-loam and loamy-sand types, which have a permeability range of $10^{-13}-10^{-11}$ m^2.

Soil-gas entry into the house was measured by a tracer-gas technique similar to that of Nazaroff (*10*). Sulfur hexafluoride was injected into the soil in a number of probes on the north and west sides of the house. One month later, SF_6 was detected in the soil gas at all probes. Dichlorofluoromethane (Freon-12) was also distributed throughout the soil, apparently having migrated onto the site from the adjacent municipal landfill. Both compounds were detected by on-site gas chromatography.

After the basement was purged with fresh surface air, it was sealed and depressurized by blower door. Soil-gas entry rates were determined by monitoring basement concentrations of SF_6 and Freon-12 while incrementally increasing basement depressurization. Soil gas entry into the house was estimated from the experimental data by using a simple mass balance model. A number of factors combine to introduce considerable uncertainty into this estimate. First, the soil-gas tracers were inhomogeneously distributed in the soil. Although the highest concentrations of both tracers appeared in samples taken from beneath the basement floor, above floor level SF_6 had higher concentrations on the west side of the house, and Freon-12 had higher concentrations on the north and east sides. Furthermore, our knowledge of the distributions of both tracers and of the permeability of the soil was limited by the number and locations of the soil probes. In addition, the actual leakage geometry of the basement was unknown. It was therefore difficult to characterize the precise source and concentration of tracer gas entering the basement. As a result, the technique was only able to give an approximate estimate of entry rate. At a basement depressurization of 30 Pa, the best estimate of the rate of entry of soil gas into the basement was 4 m^3 h^{-1}, with a possible range of 1.5–12 m^3 h^{-1}.

Model Description

Flow of soil gas through unsaturated soil (at driving-force pressures induced in the field experiment and under normal house operating conditions) obeys Darcy's law of flow through porous media (*4, 21*). Darcy's law for the pressure-driven flow of soil gas is written

$$v = -k/\mu \nabla P \tag{1}$$

where v is the volumetric fluid flux, k is the permeability of the soil to air, μ is the viscosity of soil gas (taken as the viscosity of air), and P is the disturbance pressure (total pressure minus atmospheric pressure).

To model the soil-gas response to basement depressurization, we used a standard two-dimensional, steady-state finite element model of fluid flow through porous media. The model was run on an IBM PC AT. Such models are in common use to solve groundwater flow problems (*22*). These models apply Darcy's law across each element under the constraints imposed by the user-defined boundary conditions. (The rapid attainment of steady-state soil pressures observed in the field after imposed changes in basement pressure indicated that a steady-state model was applicable.)

The field site was modeled by taking an east–west cross section at the midpoint of the basement. All model boundaries were designated as flux boundaries, with the soil surface and the interior of the basement wall and floor designated as constant pressure boundaries. The modeled region was terminated 42 m to the west of the house and 8.5 m below the soil surface to ensure that pressure predictions within the probe field region would be insensitive to boundary effects. The basement wall and floor were incorporated as elements in the flow net and assigned a thickness of 0.25 m. To minimize the computational effort, variable-sized elements were used. Finer mesh was used to define the basement walls and floor and the probe field region. Coarse mesh was used in outlying areas, thereby limiting the total number of nodes to 196.

To mimic conditions of the tracer-gas entry experiment, all cases of the model were run with soil surface and basement interior pressures of zero and −30 Pa, respectively. Since the percentage of the basement pressure seen by the soil is unchanged by the choice of basement pressure, the modeling predictions, expressed as fractional depressurizations, could be compared with pressure-field measurements, which were made at −25 Pa. The gas flow predictions, which do vary with basement pressure, were compared directly with tracer-entry measurements made at −30 Pa.

A sensitivity analysis was performed to determine the size of the error that might result from the changes in aspect ratio in adjacent elements due to the use of variable-sized elements in the mesh. A close-up of the basement wall region was modeled with the flow net terminating 7 m west of the wall and 4.3 m below the floor. The model was run twice, once with high-resolution soil elements (167 elements total) allowing only small changes in size and aspect ratio of adjacent elements and once with the wall and soil elements as they were in the main modeling effort (49 elements total for this region). The deviation between the fine and coarse mesh predictions was less than 5% out to 2.5 m west of the house and less than 10% beyond 2.5 m. Much of the deviation between the close-up models beyond 2.5 m is explained by boundary effects, as determined by comparing the results of the main modeling effort with those of the identical, close-up model. Therefore, the estimated uncertainty due to the use of variable-sized elements in the main modeling is probably less than 5% out to the D row and is certainly less than cracks in the building substructure (*10, 12–15*).

Although pollutant transport through permeable substructure walls has been considered in the context of radon entry into residential buildings (*16, 17*), to our knowledge, porous walls have not been incorporated in contaminant entry and exposure assessment modeling. Marynowski (*18*) and Harris et al. (*19*) conducted laboratory studies of air flow through cement-block walls. Their results indicate that significant air flow can occur through this type of wall, even at low pressure differentials. Marynowski measured an air flow rate of 1.3×10^{-5} m s^{-1} (13 cm^3 s^{-1} per m^2 of wall area) for uncoated, hollow cement-block wall at an applied pressure difference across the wall of 10 Pa and measured a flow rate of 1.3×10^{-6} m s^{-1} (1.3 cm^3 s^{-1} per m^2) for hollow cement-block wall sealed with a mortar coating. Harris et al. measured a flow rate of 1.6×10^{-4} m s^{-1} (160 cm^3 s^{-1} per m^2) for uncoated, hollow wall at a 1-Pa pressure difference under similar experimental conditions. The difference was probably due to different physical characteristics of the cement blocks or mortar material in the different experiments.

Numerical (computer) and analytical (closed form) models have been developed to predict pressure coupling between a basement and the surrounding soil and to predict soil-gas and radon entry (*10, 13–15*). These models restrict the soil-gas entry pathway to a gap at the basement wall–floor interface. This treatment arises because, in many cases, a basement is constructed by pouring a cement-slab floor inside a previously constructed cement footer or frame. Upon drying, slab shrinkage produces a peripheral gap. The peripheral-gap geometry has also been used to represent entry through a perimeter drain-tile system connected to a basement sump through an untrapped pipe (*12*). Most of these models assume unsaturated, homogeneous, isotropic soil (*10, 13, 15*). The Loureiro (*14*) model allows different soil properties to be assigned to regions of soil adjacent to the basement wall and floor (areas frequently modified during house construction). Nazaroff et al. (10) used an analytical model based on an electrical analogue to simulate pressure coupling induced by artificial basement depressurization at a field-study house. The model underpredicted the measured values by more than a factor of 10. The authors hypothesized that their predictions might be low due to layering of dissimilar soils, a factor for which their simple analytical model could not account.

In this paper we summarize field evidence and present the results of modeling of soil-gas entry into a house with a basement via permeable substructure walls. This work was part of a larger study on the soil-gas source and entry of volatile organic contaminants into a house. See also ref 6. The permeable wall approach was first considered because basement construction of the study house was not of the type likely to produce a gap at the wall–floor interface, and no evidence of such a gap was observed. The slab and footer of the study house were poured as one piece. The concrete block wall was then built on top of the footer. Water damage on a large section of the interior walls indicated that gas flow across the walls could be possible.

A two-dimensional, steady-state finite element model of fluid flow through porous media is used to simulate the conditions of the field experiments. The soil is modeled both with and without a low-permeability soil layer just above the depth of the basement floor (as indicated by field observations). The results of the modeling are compared with field measurements of the pressure coupling between the basement of the house and the surrounding soil and

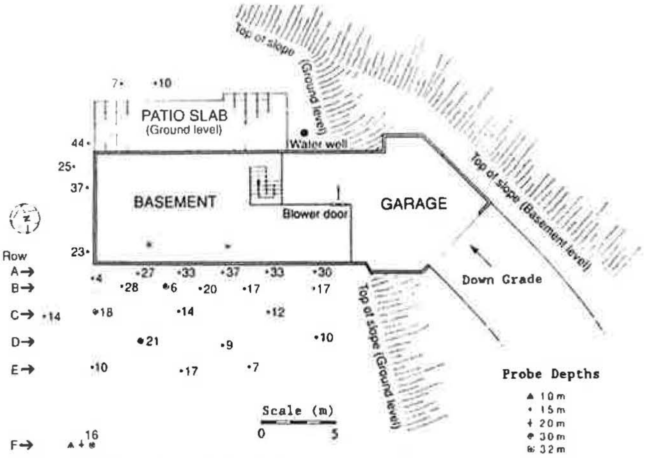

Figure 1. Plan view of the field site showing the basement-level floor plan and soil probe locations. Pressures measured at the probes are given in percent of basement depressurization. All probe depths are relative to first-floor ground level. Environmental noise is the dominant source of uncertainty in these measurements. Uncertainty was less than or equal to 30%, with an average uncertainty of 21%, for all except for four probes. The two east-side probes had uncertainties of 70 and 100%, and two of the A-row west-side probes had uncertainties of 39 and 75%. For greater detail see Garbesi (ref 20, p 42).

with data on soil-gas entry into the basement. The difference in potential for soil-gas entry through permeable walls versus entry through a perimeter gap are examined by comparing the results of the present model with predictions from the perimeter gap models of Loureiro (*14*), Mowris (*13*), and Mowris and Fisk (*15*).

Field Measurements

The study site was a unoccupied, single-family residence located in central California. The site is level to the north and west, but slopes abruptly down from the house on the south and southeast (Figure 1). The house is a three-bedroom, one-story structure built over a basement and garage, which terminate at a depth of 2.5 m below grade. The basement walls were constructed of hollow cement blocks and then backfilled with cement and coated with an asphalt sealant on the exterior. The interior walls and floor of the basement were painted, but otherwise bare. The floor areas of the first floor and basement are 183 and 103 m^2, respectively. A complete description of the study site and field measurements may be found in Hodgson et al. (*6*). The results are briefly summarized here.

Pressure coupling between the basement and the surrounding soil was measured by using the technique of Nazaroff et al. (*10*). With the basement of the study house depressurized by blower door (large fan) to 25 Pa below atmospheric, pressures were measured in soil probes distributed around the house at depths ranging between 1.0 and 3.2 m. The majority of the measurements were made on the west side of the house because of easier access to the soil surface and because the source of volatile organic soil contaminants, measured at the soil probes for another part of the larger study, was believed to be a landfill located adjacent to and west by northwest of the study site.

Figure 1 indicates the measured pressure coupling (in percent of basement underpressure) at the probe locations. Pressure coupling was fairly evenly distributed about the house. This is in contrast to earlier field research, which found pressure coupling to be highly localized to holes or cracks in the building substructure (*10, 3*). Coupling on the west side of the house was generally observed to be between 30 and 37% for probes 0.5 m from the basement wall and 1.5 m deep. Coupling decreased smoothly with